Dissolution and Precipitation Behavior of Amorphous Solid Dispersions

DAVID E. ALONZO,[1,2] YI GAO,[2] DELIANG ZHOU,[3] HUAPING MO,[4] GEOFF G. Z. ZHANG,[2] LYNNE S. TAYLOR[1]

[1]Department of Industrial and Physical Pharmacy, College of Pharmacy, Purdue University, West Lafayette, Indiana 47907

[2]Global Pharmaceutical Research and Development, Abbott Laboratories, Abbott Park, Illinois 60064

[3]Global Pharmaceutical Operations, Abbott Laboratories, North Chicago, Illinois 60064

[4]Department of Medicinal Chemistry and Molecular Pharmacology, Purdue Interdepartmental NMR Facility, College of Pharmacy, Purdue University, West Lafayette, Indiana 47907

Received 3 January 2011; revised 28 March 2011; accepted 31 March 2011

Published online 23 May 2011 in Wiley Online Library (wileyonlinelibrary.com). DOI 10.1002/jps.22579

ABSTRACT: Amorphous solid dispersions (ASDs) are widely utilized in the pharmaceutical industry for bioavailability enhancement of low solubility drugs. The important factors governing the dissolution behavior of these systems are still far from adequately understood. As a consequence, it is of interest to investigate the behavior of these systems during the dissolution process. The purpose of this research was twofold. First, the degree of supersaturation generated upon dissolution as a function of drug–polymer composition was investigated. Second, an investigation was conducted to correlate physical behavior upon dissolution with polymer loading. Felodipine and indomethacin were selected as model drugs and hydroxypropylmethylcellulose (HPMC) and polyvinylpyrrolidone (PVP) were used to form the dispersions. Diffusion and nuclear magnetic resonance spectroscopy experiments revealed that the extent of bulk supersaturation generated on dissolution of the ASD did not depend on the drug–polymer ratio. Interestingly, the maximum supersaturation generated was similar to the predicted amorphous solubility advantage. However, dynamic light scattering measurements revealed that particles on the submicron scale were generated during dissolution of the solid dispersions containing 90% polymer, whereas solid dispersions at a 50% polymer loading did not yield these nanoparticles. The nanoparticles were found to result in anomalous concentration measurements when using *in situ* ultraviolet spectroscopy. The supersaturation generated upon dissolution of the solid dispersions was maintained for biologically relevant timeframes for the HPMC dispersions, whereas PVP appeared to be a less effective crystallization inhibitor. © 2011 Wiley-Liss, Inc. and the American Pharmacists Association J Pharm Sci 100:3316–3331, 2011

Keywords: felodipine; indomethacin; amorphous; solid dispersion; supersaturation; polymer; dissolution; crystallization inhibition

INTRODUCTION

Amorphous solid dispersions (ASDs) are of great current interest as a formulation strategy for increasing the effective solubility[1–4] and bioavailability[5–9] of insoluble active pharmaceutical ingredients (APIs). However, the fundamental processes that govern the dissolution of ASDs are not well understood, making scientifically sound formulation design challenging from a dissolution and performance perspective. Simonelli et al.[4] illustrated a number of complexities that need to be considered when evaluating the dissolution behavior of solid dispersions including the drug–polymer ratio, the relative dissolution rates of the two components, and the crystallization behavior of the drug during the dissolution process.

Much of the research conducted in the area of solid dispersion dissolution has focused on evaluating differences in dissolution rates between various systems/compositions. An additional parameter that has not been widely studied is the degree of supersaturation generated and maintained following

Correspondence to: Lynne S. Taylor (Telephone: +765-496-6614; Fax: +765-494-6545; E-mail: lstaylor@purdue.edu), Geoff G. Z. Zhang (Telephone: + 847-937-4702; Fax: + 847-937-7756; E-mail: geoff.gz.zhang@abbott.com)

Journal of Pharmaceutical Sciences, Vol. 100, 3316–3331 (2011)

dissolution under nonsink conditions. Thus, one important question that remains largely unaddressed is: how does the "solubility advantage" (here we use the term coined by Hancock and Parks[1] to describe the transient concentration enhancement potentially offered by amorphous solids) of the amorphous dispersion compare with that obtained from the pure amorphous drug? It is difficult to predict/measure the solubility advantage of a pure amorphous solid for both thermodynamic (a glassy amorphous solid is a nonequilibrium form, so from a rigorous thermodynamic perspective, it is impossible to measure/define a solubility value) and kinetic reasons (rapid crystallization to a more stable form). Recent studies have highlighted some of the considerations that need be taken into account when predicting and evaluating the dissolution behavior of amorphous solids.[10–12] It has been shown that the physical stability of the pure amorphous solid against crystallization when in contact with the dissolution medium, as well as the crystallization kinetics of the supersaturated solution generated via dissolution, are important factors that dictate the observed concentration–time profiles.[10] When both the amorphous solid and the supersaturated solution can be stabilized against crystallization, the maximum supersaturation observed can reach a level that is close to the theoretically estimated amorphous solubility. Although concentration–time profiles are commonly measured for amorphous solids, the magnitude of the observed supersaturation is not always compared with theoretical estimates. This comparison is important as it not only provides an inherent "measuring stick" from which to gauge the performance of the amorphous solid but can also serve as an indicator of the stability (or lack thereof) of the supersaturated solution and/or amorphous solid. With the understanding of the origin of a particular instability, we can seek strategies to improve the stability of these systems and maximize the advantage gained from using a high-energy form.

The theoretical solubility advantage that would be expected following dissolution of an amorphous solid can be estimated by several different methods.[1,11,13,14] The underlying assumption of all of these calculations is that the difference in free energy between the crystalline and amorphous form is responsible for determining the maximum possible theoretical solubility advantage. The free energy difference between a crystalline material and the supercooled liquid can be estimated from the melting temperature and enthalpy of fusion, however, this method becomes increasingly approximate if the operating temperature is much below the glass transition temperature (T_g).[13] If the configurational heat capacity is known, a more rigorous estimate can be made where the proximity of the operating temperature to the T_g is less of an issue.[14,15] Murdande et al.[11] have published a more sophisticated model that, in addition to calculation of the energetic differences, takes into account changes in activity due to both water absorption and differing extents of ionization of the crystalline and amorphous forms. These corrections can be significant for acidic or basic compounds, or if the amorphous form absorbs a significant amount of water. Regardless of the method used for estimating the solubility advantage, the main driver remains the difference in free energy between the amorphous and crystalline forms. It is important to note that all of these estimations assume that the contribution of the solute–solvent intermolecular interactions to the solubility remains the same, regardless of whether the solid is in the amorphous state or the crystalline state. Although this assumption is reasonable for the comparison of a poorly soluble stable crystalline form with its pure amorphous form (or metastable polymorphs), it is of interest to consider how this would apply to an ASD. Assuming the presence of intermolecular interactions between the API and the polymeric carrier, it would be reasonable to speculate that the theoretical estimates described above would not be applicable to ASDs. Dissolution of an API dispersed in a polymeric matrix is known to be affected by both the type of polymer as well as the relative drug-to-polymer composition.[3,4,16] Other contributing factors summarized in the literature include polymer–drug miscibility, physical stability of the solid dispersion, and aqueous solubility of both components.[17,18]

Dissolution of ASDs has been shown in many instances to yield higher solution concentrations than that of the crystalline form or the pure amorphous form.[19,20] However, the underlying behavior that yields the concentration–time profiles could be extremely complex, requiring a deeper understanding in order to fully characterize such systems. The purpose of this study was to investigate the behavior of ASDs containing felodipine or indomethacin incorporated in different polymeric carriers at various drug loadings during dissolution under nonsink conditions. The progression of solution concentration–time profiles was monitored using ultraviolet (UV) spectroscopy and diffusion experiments, whereas precipitation behavior was investigated using dynamic light scattering (DLS). Cross-polarized light microscopy was also used to visualize the dissolution of the ASDs. Solution nuclear magnetic resonance (NMR) spectroscopy was employed to verify the degree of supersaturation produced by felodipine ASDs.

MATERIALS

Felodipine was provided by AstraZeneca, Södertälje, Sweden. Indomethacin was purchased from Hawkins Pharmaceutical (Hawkins Inc., Minneapolis, Minnesota). Polymers used included

polyvinylpyrrolidone (PVP) K29/32 purchased from Sigma–Aldrich Company. (St. Louis, Missouri) and hydroxypropylmethylcellulose (HPMC) Pharmacoat grade 606 supplied by Shin-Etsu Chemical Company, Ltd. (Tokyo, Japan). The dissolution medium used for all experiments was 50 mM phosphate buffer (pH 6.8) for felodipine and 50 mM phosphate buffer (pH 2.0) for indomethacin.

METHODS

Preparation of ASDs

Solid dispersions of amorphous felodipine and indomethacin were prepared by dissolving the model compound and polymers in a solution of 50% methanol and 50% dichloromethane by volume, followed by rotary evaporation. Two concentrations were investigated for all drug–polymer systems in this study: 90% polymer–10% API (90:10, w/w) and 50% polymer-50% API (50:50, w/w). The miscibility of all API–polymer combinations has been previously confirmed.[21–23] Samples were cryomilled with a Spex cryomill (Model 6750; SPEX CertiPrep LLC, Metuchen, New Jersey) for 30 s at four impacts per second for four cycles in order to yield a reasonably uniform particle size. The ASDs were then stored in desiccators containing Drie-Rite® (WA Hammond Drierite Co. LTD., Xenia, OH, USA) in a refrigerator.

UV Spectroscopy

Dissolution and diffusion experiments were carried out using an Ocean Optics 6 channel *in situ* UV–Vis fiber optic system (Dunedin, Florida). Wavelength scans were performed at 1 min time intervals for all experiments and in the interests of clarity, some data points were excluded from the graphs presented in the *Results* section. Absorbance values from 270 to 450 nm were used for analysis. Second derivatives of the spectra were taken for both the calibration and investigation sample data in order to mitigate particle scattering effects. Calibration solutions were prepared in pure methanol for both APIs investigated. Dissolution media containing stir bars (+ shaped) rotating at 300 rpm were equilibrated at 37°C or 25°C prior to addition of the solid dispersions. API (either as an ASD or predissolved in methanol) was then added to 18 mL of dissolution medium and data collection commenced immediately. For analysis of the solid dispersion samples, approximately 5–20 mg of solid was introduced to the dissolution medium depending on the drug-to-polymer ratio. For all samples, dissolution was performed under nonsink conditions in order to assess the maximum achievable solution concentration. In the case of the solid dispersions, all polymers present in the solution was derived solely from the initial solid added. Use of phrase "nominal concentration" with respect to solid dispersions refers to the solution concentration that would be generated if the solid or individual components dissolved completely. When used in reference to supersaturated solutions generated by solvent addition, "nominal concentration" refers to the calculated concentration added through pipetting prior to any precipitation. Diffusion experiments where felodipine predissolved in methanol was used to generate supersaturated conditions contained HPMC predissolved in the buffer. See *Diffusion Experiments* section below for details. All experiments except the 90:10 HPMC-felodipine solid dispersion dissolution at 37°C with different amounts of solid were performed in triplicate.

Diffusion Experiments

In order to investigate the accuracy of observed differences in peak solution concentrations of felodipine from the dissolution experiments, diffusion experiments through dialysis tubing were performed at 37°C with various supersaturated solutions of felodipine. Differences in diffusion–flux across a dialysis membrane can be described by the following equation[24]:

$$J_{\mathrm{i}} = \frac{D_{\mathrm{i}} \times K_{\mathrm{i}}}{l} \times (c_{\mathrm{io}} - c_{il}) \qquad (1)$$

where J_{i} is the flux of component i across a dialysis membrane, D is Fick's law diffusion coefficient, K is the sorption coefficient for the liquid/membrane phase, l is the thickness of the membrane, and $(c_{\mathrm{io}} - c_{il})$ is the difference in concentration between outside and inside of the membrane. Therefore, flux across a dialysis membrane will be directly proportional to the concentration difference across membrane. Consequently, any significant difference in the level of the supersaturation between various solid dispersions will be directly reflected as difference in the flux across the membrane.

A 600 mL-jacketed beaker with a stir bar was filled with 300 mL of dissolution buffer (pH 6.8 50 mM phosphate). A UV fiber optic probe (as described above) was inserted into the vessel, which will be referred to as the donor chamber. A second chamber, termed the receptor chamber, consisted of a second UV probe placed in dialysis tubing containing 10 mL of pH 6.8 buffer. This solution contained 500 μg/mL of predissolved HPMC added to prevent crystallization of the drug following diffusion into the receptor compartment. The dialysis tubing was purchased from Spectrum Laboratories Inc. (Rancho Dominguez, California), and was Spectra/Por1 membrane type with a flat width of 32 mm and a molecular weight cutoff of 6–8 kDa. Figure 1 shows a schematic of the general experimental setup.

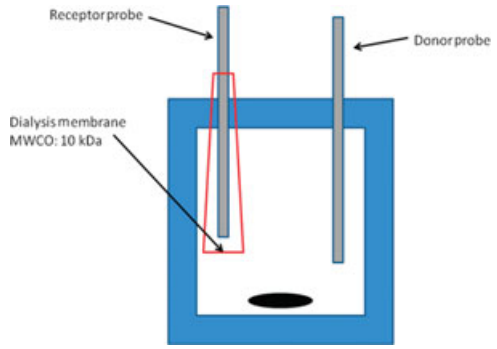

Figure 1. Experimental schematic for the diffusion experiments.

Supersaturated solutions were generated by two different methods. First, solid dispersions containing 90:10 or 50:50 HPMC–felodipine, or pure amorphous felodipine were placed into the donor chamber and allowed to dissolve. Crystalline felodipine was used as a control. For the experiments with the solid dispersions, all of the dissolved polymer present in the donor chamber originated from the solid. In the case of the pure amorphous felodipine and crystalline felodipine, HPMC was predissolved at a solution concentration of 250 μg/mL. Second, two additional control experiments were conducted, whereby supersaturated solutions of felodipine were produced by pipetting into an aqueous buffer (pH 6.8), a concentrated methanolic solution of felodipine generating nominal solution concentrations of 5 and 10 μg/mL. As with the pure amorphous felodipine and crystalline felodipine, HPMC was predissolved in the dissolution medium at a concentration of 250 μg/mL. The receptor chamber was initially kept separate from the donor chamber for experiments with all solid samples in order to allow a stable solution concentration to be generated by the dissolution process. Solid was thus introduced and allowed to dissolve until a plateau in the concentration was reached according to the donor probe measurements. This was approximately 40 min for the amorphous samples and about 60 min for the crystalline sample. Once this steady state was reached, the diffusion chamber was introduced to the donor chamber and the concentration in each chamber was measured as a function of time. When the supersaturation was generated by adding a concentrated methanolic solution of the drug, the receptor chamber was present in the donor chamber from the beginning of the experiment as the maximum supersaturation level was instantaneous. The receptor chamber was set up immediately prior to use in order to ensure that the membrane did not dry out. The membrane was kept in a beaker with deionized water and the receiving solution was preheated to 37°C prior to use. The slopes of the concentration–time profiles obtained from the receptor chamber were used to estimate diffusion rates. All experiments were performed in triplicate.

Dynamic Light Scattering

Dynamic light scattering experiments were performed using a Malvern Zetasizer ZS® (Worchestershire, UK) series instrument. A 173° backscatter detector was used in order to minimize the signal from large dust particles or other large contaminants. For the majority of the experiments, the measurement settings were optimized automatically by the Malvern Zetasizer® software. However, two experiments were conducted with the measurement position and attenuation manually set to 1.25 mm and 6, respectively, to measure the relative amount of particles present in different systems. These parameters must be set to the same values for each experiment to properly compare particle concentration from different samples using scattering intensity. Disposable cuvettes purchased from VWR International (West Chester, Pennsylvania) with a 1 cm path length were used as sample containers. Experiments were performed at 25°C and 37°C and under similar conditions to the dissolution experiments with respect to the dissolution media, stirring rate and concentrations of the API. Briefly, supersaturated solutions of felodipine or indomethacin were generated by dissolution of solid dispersions or by pipetting methanolic solutions of drug into the dissolution buffer. In the case of the solid dispersions, all polymers present in the solution was derived solely from the initial solid added. When the methanolic solutions were used to create supersaturation, polymer was predissolved in the buffer prior to the start of the experiment.

Optical Microscopy

A Nikon Eclipse E600 Pol microscope with a 10× or 20× objective was used with NIS-Elements software package (Version 2.3; Nikon Company, Tokyo, Japan). ASDs were analyzed using polarized light with the analyzer at 90° with respect to the polarizer and a λ (530 nm) tint plate at room temperature. The ASD particles were placed on a microscope slide and then exposed to phosphate buffer. Images were taken at various time intervals in order to observe the physical behavior of these systems. Select images are presented in the *Results* section.

Solution NMR Spectroscopy

Proton NMR spectroscopy (solution)[25] was used to compare the maximum degree of supersaturation generated by dissolution of a 90:10 and a 50:50 (HPMC–felodipine) ASD. Dissolution experiments with these solid dispersions (90:10 and 50:50) at 37°C, carried out exactly as described above in the *UV Spectroscopy* section, were performed. NMR samples were prepared for both systems by combining

20 μL D_2O with 530 μL of suspension in NMR tubes withdrawn from the dissolution vessel using a micropipettor, 50 min after the start of the experiment. One-dimensional (1D) proton NMR data acquisitions commenced within 30 min of sample preparation at 37°C using a Bruker AVANCE DRX500 spectrometer equipped with an inverse proton cryoprobe and single-axis (z) gradient. Successive 1D proton solution spectra were monitored over approximately 40–60 min to determine the relative solution concentration of felodipine generated by dissolution of the 90:10 and 50:50 solid dispersions, with each spectrum accumulated over 256 scans. The total interscan delay was 5 s, sweep width was 16 ppm, and 16 K complex data points were acquired. Solvent water was suppressed by a WATERGATE sequence so that the aromatic signals of felodipine could be clearly observed. Aromatic peaks of felodipine were integrated to determine the relative solution concentration after the free induction decay was processed with a mild window function (0.3 Hz exponential line broadening), Fourier transformation, manual phasing, and baseline corrections.

Estimation of the Amorphous Solubility Advantage

In order to approximate the solubility ratio of the pure amorphous to crystalline form, Eq. 2 was used[1]:

$$\frac{\sigma^{\text{amorph}}}{\sigma^{\text{crystal}}} = e^{\frac{\Delta G}{RT}} \tag{2}$$

where $\sigma^{\text{amorph}}/\sigma^{\text{crystal}}$ represents the ratio of the solubility of the amorphous form to the solubility of the stable crystalline form. ΔG is the free energy difference between the amorphous and crystalline forms, R is the universal gas constant, and T is the temperature in Kelvin. The free energy difference estimate is obtained from the Hoffman equation.[13]

$$\Delta G = \frac{\Delta H_f \times \Delta T \times T}{T_m^2} \tag{3}$$

where ΔH_f is the enthalpy of fusion, T is the operating temperature, T_m is the melting temperature, and ΔT is $T_m - T$. Enthalpies of fusion were measured using a TA Q2000 differential scanning calorimeter (TA Instruments, New Castle, Delaware) and analysis of the melting endotherms was performed using the TA Universal analysis software. Solubility values of the α crystalline form of indomethacin were measured in pH 2.0 dissolution media in the presence and absence of predissolved polymer using UV spectroscopy for analysis of the solution concentration. The presence of the polymers at the aforementioned concentration did not have an impact on the equilibrium solubility at either 25°C or 37°C. The equilibrium solubility values for felodipine were taken from Konno et al.[2]

RESULTS

Dissolution of Felodipine ASDs

Figure 2 shows the apparent concentration–time profiles, generated from the absorbance values measured using a UV dip probe during dissolution of felodipine–HPMC ASDs at 37°C. When 90% (w/w) of the solid dispersion is HPMC, the apparent solution concentration of felodipine peaked between 25–30 μg/mL, which was approximately 100% of the total amount of felodipine present in the solid initially introduced to the dissolution medium (30 μg/mL). When the polymer-to-drug ratio was reduced to 50:50, and the same mass of ASD added, the solution concentration of felodipine peaked at around 9 μg/mL despite the fact that there was more felodipine (150 μg/mL) in the system. This peak was close to the theoretically estimated solubility of the pure amorphous form (~9.1 μg/mL) and well below the total amount of felodipine added to the solution. It can be further noted that the measured rate of dissolution of the 90:10 HPMC–felodipine ASD was much faster than that of the 50:50 HPMC–felodipine ASD. Figure 3 shows the apparent concentration–time profiles obtained when increasing amounts of the 90% HPMC solid dispersion were added to the dissolution medium. As the amount of solid (and therefore felodipine) was increased, the peak solution concentration observed also appeared to increase, with the maximum occurring within the first 10 min of the experiment. Similar to the 90:10 samples shown in Figure 2, the apparent peak concentration achieved was 80%–100% of the total amount of felodipine introduced to the dissolution medium for all three samples. Interestingly, these solutions become uniformly

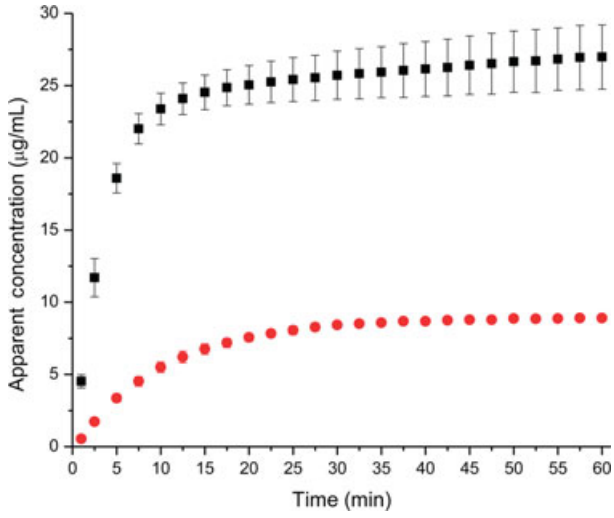

Figure 2. Apparent dissolution profiles of 90:10 (■) and 50:50 (●) HPMC–felodipine solid dispersions at 37°C. Error bars represent 1 standard deviation (n = 3).

 DOI 10.1002/jps

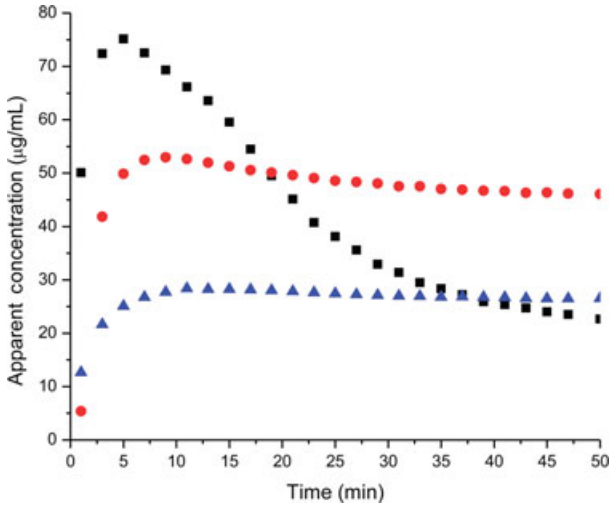

Figure 3. Apparently dissolution profiles at 37°C for 90:10 HPMC–felodipine solid dispersions containing 90 (■), 60 (●), and 30 μg (▲) felodipine per mL of dissolution buffer.

cloudy a few minutes after the solid was introduced to the solution. This cloudiness was only visually observed during dissolution of the 90% HPMC solid dispersions. When the 50% HPMC systems were investigated, individual particles (assumed to be initial dispersion particles) were visually detectable. Uniform cloudiness was not observed.

Qualitative differences in dissolution behavior of the two ASDs could be observed using cross-polarized microscopy. Figure 4 shows images from experiments where both the 90:10 and 50:50 HPMC–felodipine solid dispersions were exposed to dissolution buffer and analyzed under cross-polarized light. Interestingly, in the case of the 90% HPMC ASD, the initial structure of the particle dissipated very rapidly (within 5 min). In contrast, the particles made up of 50:50 HPMC–felodipine maintained their initial shape and integrity for at least 30 min. PVP–felodipine solid dispersion behavior was visually consistent with what was observed for the HPMC–felodipine solid dispersions (data not shown). Particles from the 90% PVP ASD disappeared almost instantly, whereas the particles from the 50% PVP ASD remained intact throughout the experiment.

To evaluate any temperature-dependent effects, a second set of dissolution experiments was performed at 25°C (Fig. 5). Similar to 37°C, very high apparent supersaturations were measured at 25°C upon dissolution of the ASDs containing 90% HPMC. However, when the 50:50 HPMC–felodipine ASD was dissolved, the peak solution concentrations were much lower, reaching a maximum just above the theoretically predicted solubility of amorphous felodipine of 5–6 μg/mL. Both 90:10 and 50:50 PVP–felodipine ASDs were also investigated at this temperature, and similar to the ASDs containing HPMC, dispersions containing 90% polymer (PVP) resulted in very high apparent solution concentrations. Again, the initial dissolution rates are much faster in the 90% PVP ASD than in the 50% ASD. These results, in combination with the data obtained at 37°C indicate that the relative amount of polymer-to-drug in the ASD was an extremely important factor in determining the dissolution behavior. As with the experiments conducted at 37°C, the dissolution

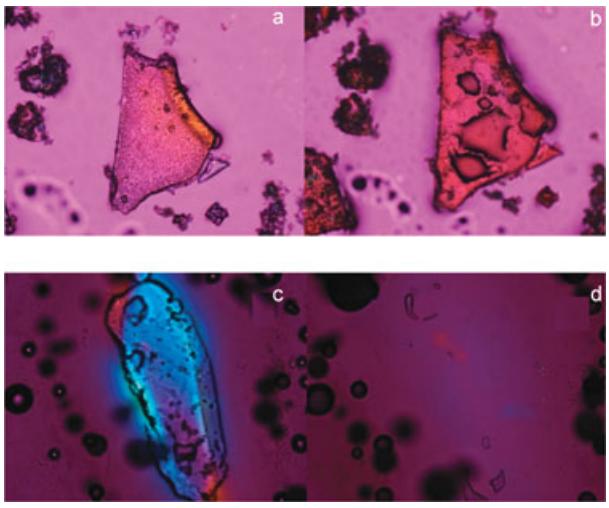

Figure 4. Solid dispersion microscope images under cross-polarized light: 50:50 HPMC–felodipine (10× magnification) initial (a) and 30 min after exposure (b), and 90:10 HPMC–felodipine (20× magnification) initial (c) and 5 min (d) after exposure.

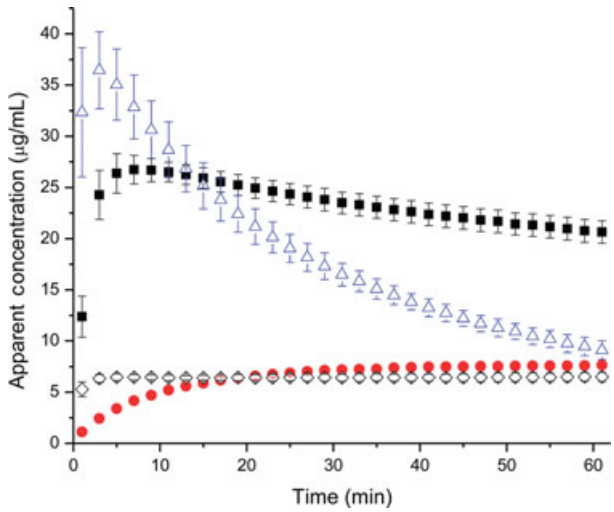

Figure 5. Apparent dissolution profiles of 90:10 HPMC–felodipine (■), 50:50 HPMC–felodipine (●), 90:10 PVP–felodipine (Δ), and 50:50 PVP–felodipine (◊) solid dispersions at 25°C. Error bars represent 1 standard deviation ($n = 3$). Error bars for the 50:50 data are smaller than the symbols.

medium became uniformly cloudy within a few minutes only for the samples containing 90% PVP.

Dynamic Light Scattering

The observed cloudiness in the previous section indicated that there were very small scattering particles present in the solutions generated during dissolution of the 90:10 ASDs (PVP or HPMC). DLS was used to evaluate the size of these scattering particles as well as to monitor any changes in diameter as a function of time. Figure 6 shows the particle size as a function of time in a system where the scattering particles were generated by dissolution of a 90:10 (HPMC–felodipine) solid dispersion at 25°C. The nominal amount of felodipine present in the system was 25 μg/mL (analogous to the system shown in Fig. 5). Initially, the average particle diameter was around 215 nm and increased to above 300 nm after 90 min. Further observation of the particle size evolution indicated that these particles continued to grow over an experimental period of 10 h. Around the 10^{th} h, there was a substantial jump in particle size, which most likely results from the fact that a significant portion of the particles present in the solution had grown to above a micrometer in diameter. As a consequence, many of the particles in the suspension were too large for Brownian motion to overcome the force of gravity and began to settle out. The presence of large particles settling in a solution can cause inaccuracies in the calculation of particle size from the autocorrelation function even when a backscattering detector is used. Nevertheless, this measurement can still provide an approximate indication of the particle size. Settling was indeed visually observed for this sample, whereby accumulation of particles at the bottom of the sample cell could be seen after allowing the material to settle for 5–10 min. To confirm the visual observations from the dissolution experiments, sufficient 50:50 (HPMC–felodipine) solid dispersion was added to the dissolution medium to generate a nominal felodipine concentration of 250 μg/mL and analyzed for submicron particles. On the basis of examination of the correlation function, no submicron particles could be detected in the system and were therefore assumed to be absent.

Additional experiments were conducted to further explore this phenomenon, evaluating the size of the submicron particles formed in the supersaturated solutions generated by dissolution of ASDs as well as supersaturated solutions generated through adding a methanolic solution of the drug. For these studies, we chose to add different masses of the 90:10 HPMC–felodipine ASD to 20 mL of dissolution buffer to generate a nominal felodipine solution concentration of either 30 or 50 μg/mL. The nominal HPMC concentrations in these solutions were 270 and 450 μg/mL, respectively. For comparison, supersaturated solutions were created by adding a methanolic solution of felodipine to generate nominal felodipine concentrations of 30 and 50 μg/mL. HPMC was predissolved in these solutions at concentrations of 250 and 500 μg/mL, similar to the ASD systems described above. Particle size as a function of time in the above systems was monitored and the resultant comparisons are shown in Figure 7. In all instances, submicron particles were generated, which increased in size with time, rapidly at first and more slowly later. Interestingly, both the initial size of the particles and their evolution with time was very similar for these different systems, where the initial particle size was

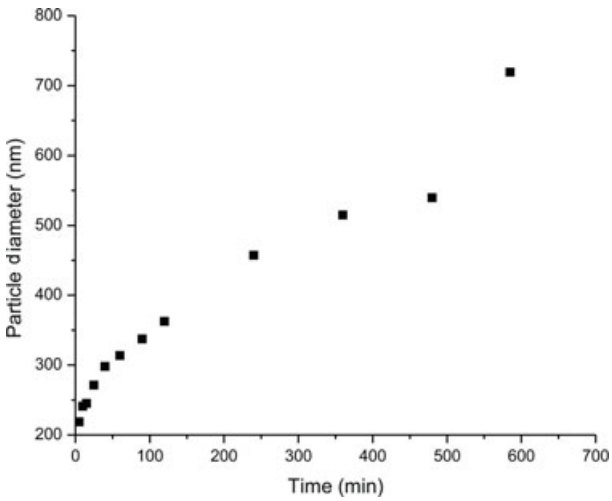

Figure 6. Average particle diameter generated during dissolution of a 90:10 (HPMC–felodipine) solid dispersion at 25°C.

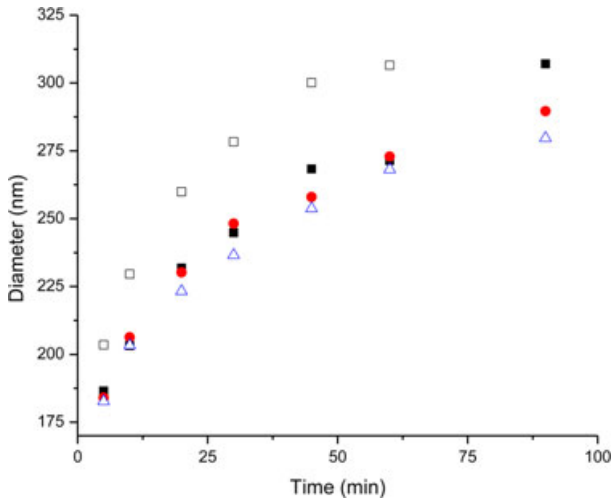

Figure 7. Average particle diameter generated by a 90:10 HPMC–felodipine solid dispersion at 30 (■) and 50 μg/mL (●), and an artificial supersaturation at 30 (Δ) and 50 μg/mL (□) at 25°C. All concentrations refer to the nominal amount of felodipine in the system.

 DOI 10.1002/jps

around 175–200 nm and increased to about 300 nm after 1.5 h. To probe if there was a difference in the concentration of scattering particles when different amounts of 90:10 (HPMC–felodipine) ASD were dissolved, experiments using the same concentrations as shown in Figure 7 were repeated. In order to properly make this comparison, the instrument parameters were set as follows: the attenuation was manually set to six and the measurement position was set to 1.25 mm (previously optimized automatically by the software). The resultant data indicated that the particle size increased from approximately 210 to 270 nm for all samples taken between 10 and 45 min (similar to data shown in Fig. 7). However, the derived intensity (i.e., amount of scattered photons detected) was 71,000 ± 7500 kilocounts per second (kcps) for the 30 μg/mL sample and 148,000 ± 8100 kcps for the 50 μg/mL sample (average and standard deviation of the data collected at 10, 20, 30, and 45 min.) As expected, the number of counts in the higher concentration sample was approximately twice that of the lower concentration sample, indicating that there was roughly twice the amount of scattering particles in the former system.

The data generated from the experiments conducted with the two different amounts of the 90:10 HPMC–felodipine ASDs (Fig. 7) were then compared with the behavior of two additional systems. First, a supersaturated solution of felodipine was artificially generated (by adding a concentrated methanolic solution of felodipine) in the dissolution medium in absence of predissolved polymer in order to evaluate the precipitation behavior in the absence of a crystallization inhibitor. The second system investigated was a solid dispersion containing 90% PVP and 10% felodipine, a polymer that has been shown to be relatively ineffective at inhibiting crystallization of felodipine from a supersaturated solution when compared with HPMC.[2,10] Figure 8 shows that the average particle size was 450 nm immediately after a solution concentration of 30 μg/mL was artificially generated in the absence of polymer at 25°C. At 7 min, the average particle size was 936 nm. At this point, the particles had grown to a size where significant settling was taking place making this measurement quantitatively unreliable. However, the fact that there were particles settling at 7 min suggests that the particles in this system grew very rapidly from the supersaturated solution in the absence of any crystallization inhibitor. In the case of the solid dispersion containing PVP, the rate of particle growth was considerably faster than in the presence of HPMC, as would be expected from previously reported data.[2,10] It should be noted that the average size at the 5 min point in the PVP ASD experiment was an outlier. This sampling point showed a bimodal distribution with a peak at about 5 μm, which can be attributed to the presence

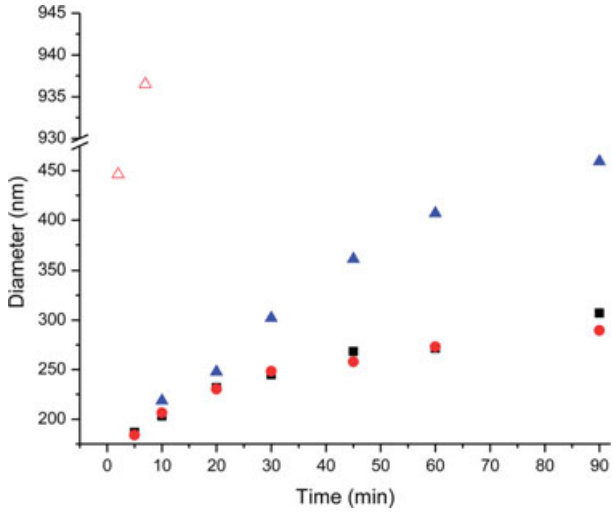

Figure 8. Average particle diameter generated by a 90:10 HPMC–felodipine solid dispersion at 30 (■) and 50 (●) μg/mL, a 90:10 PVP–felodipine solid dispersion at 40 μg/mL (▲), and an artificial supersaturation in the absence of polymer at 30 μg/mL (Δ) at 25°C. All concentrations refer to the nominal amount of felodipine in the system.

of either a dust particle or an initial solid dispersion particle not yet completely dissolved. In either case, the presence of these large particles would impact the overall average particle diameter expressed in the *z*-average hence this result was removed from the data set.

A similar set of experiments was performed at 37°C (Fig. 9), wherein the amount of felodipine added was increased because the solubility is higher than at 25°C. This was performed to ensure that there was a similar quantity of scattering particles present in the solution. For the artificially supersaturated solutions, the particle size as a function of time was almost identical to that observed at 25°C. In the case of the 90:10 HPMC–felodipine ASDs, the initial particle size generated from dissolution of the solid dispersion was consistently larger (250–260 nm) than for the same dispersion at 25°C (Fig. 8) as well as compared with the particles evolving, following artificial supersaturations at 37°C (~200 nm). The rate of increase in particle size was slower at 37°C and the profiles appear to level off faster. Consistent with the observations at 25°C, the rate of increase in size for the particles generated by dissolution of the 90:10 PVP–felodipine ASD was much higher than for the HPMC dispersion. As expected, the rate of particle growth in the absence of polymer was even more rapid.

Diffusion and NMR Spectroscopy

Because of the observation that submicron particles were generated during the dissolution of some ASD systems, it was important to verify the degree of supersaturation achieved. Diffusion and NMR

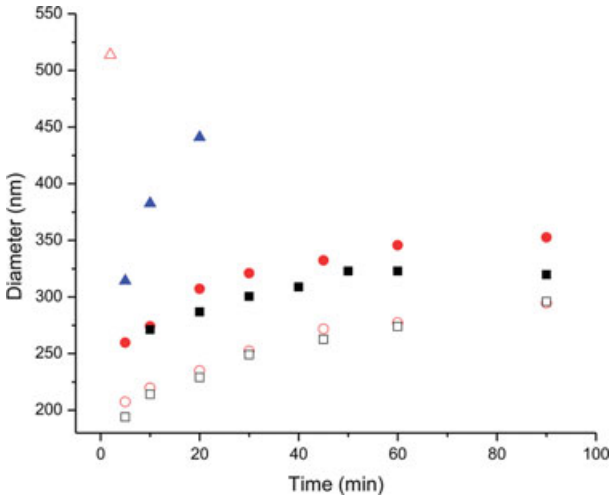

Figure 9. Average particle diameter generated by a 90:10 HPMC–felodipine solid dispersion at 40 (●) and 60 (■) μg/mL, a 90:10 PVP–felodipine solid dispersion at 50 μg/mL (▲), an artificial supersaturation in the presence of HPMC at 40 (○) and 60 (□) μg/mL, and an artificial supersaturation in the absence of polymer at 40 μg/mL (Δ) at 37°C. All concentrations refer to the nominal amount of felodipine in the system.

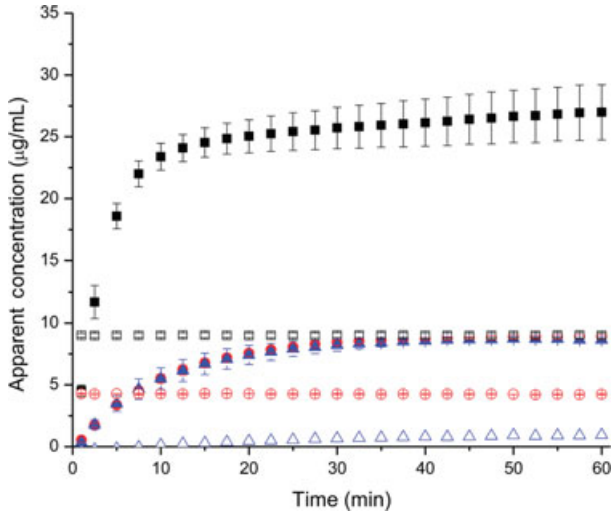

Figure 10. Apparent concentration–time profiles (donor chamber) for the dissolution of 90:10 (■) and 50:50 (●) HPMC–felodipine solid dispersions, pure amorphous felodipine (▲), and crystalline felodipine (Δ). Concentration–time profiles of artificial supersaturations of felodipine at 5 (○) and 10 (□) μg/mL. All data were acquired at 37°C. Error bars represent 1 standard deviation ($n = 3$).

experiments were therefore conducted at 37°C to determine if the apparent differences in supersaturation observed between the 90:10 and 50:50 HPMC–felodipine systems were accurate representations of the actual solution concentration or artifacts of the UV measurement. Figure 10 shows a graph of the bulk solution concentrations as a function of time for the various samples investigated, as derived from the UV measurements. As shown earlier, there was a large difference (~ factor of 2.5) in apparent maximum concentration between the 90:10 and 50:50 HPMC–felodipine ASDs. In the case of the dissolution of pure amorphous felodipine in the presence of polymer, the concentration–time profile was almost identical to that of the 50% HPMC ASD. Control experiments included artificially supersaturated solutions at 5 and 10 μg/mL (measured concentrations were slightly less) as well as a saturated solution of crystalline felodipine. According to these solution concentration versus time profiles and Eq. 1, diffusion of felodipine across a dialysis membrane from a solution generated by dissolution of the 90:10 HPMC–felodipine solid dispersion system should occur at a rate approximately 2.5 times that of the corresponding solution produced on dissolution of the 50:50 HPMC–felodipine dispersion. Furthermore, the rate of diffusion for the 5 μg/mL artificially supersaturated sample should be half of solutions produced from the 50% HPMC solid dispersion, pure amorphous felodipine, and the artificially supersaturated solution at 10 μg/mL.

Figure 11 shows the average felodipine concentration versus time profiles in the receptor chamber (error bars excluded for clarity). Visual inspection of the slopes of these profiles shows that the diffusion rate of the 10 μg/mL solution was the fastest, whereas that of the crystalline solid was the slowest. To provide a more quantitative analysis of the diffusion rates, linear regression analysis on the linear portion

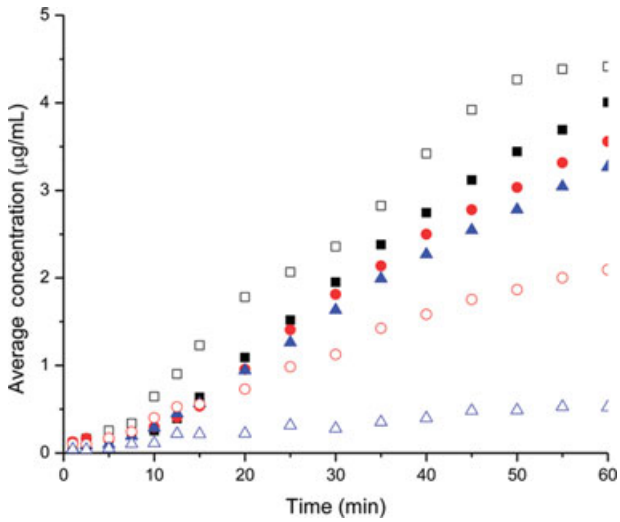

Figure 11. Diffusion profiles (receptor chamber) for the dissolution of 90:10 (■) and 50:50 (●) HPMC–felodipine solid dispersions, pure amorphous felodipine (▲), and crystalline felodipine (Δ). Concentration–time profiles of artificial supersaturations of felodipine at 5 (○) and 10 (□) μg/mL. All data were acquired at 37°C.

 DOI 10.1002/jps

Table 1. Comparison of the Relative Diffusion Rates Between ASDs, Pure Amorphous, Crystalline, and Artificially Supersaturated Felodipine ($n = 3$ except for crystalline, where $n = 1$)

System	Slope	Ratio with Crystalline Slope
10 μg/mL	0.0816 ± 0.028	10.0 ± 3.4
90:10	0.0858 ± 0.0094	10.5 ± 1.2
50:50	0.0782 ± 0.015	9.5 ± 1.8
Pure amorphous	0.0698 ± 0.015	8.5 ± 1.8
5 μg/mL	0.0394 ± 0.0032	4.8 ± 0.39
Crystalline	0.0082	1.0

(10–40 min) of the experimental data was performed to estimate the slopes of these profiles. Most systems showed a lag phase, which lasted approximately 10 min, indicating an equilibration period prior to attaining steady-state diffusion.

Table 1 summarizes values of the slopes obtained from linear regression analysis of the data. To better compare the diffusion rates between the systems, they were normalized to the slope obtained from the steady-state diffusion of a solution derived from dissolved crystalline material. The equilibrium solubility of the crystalline phase is about 1 μg/mL. When the felodipine solution concentration was artificially generated at 5 μg/mL, the rate of diffusion was 4.8 times that of the dissolved crystalline material, and when the solution concentration was generated at 10 μg/mL, the ratio of the slopes was 10. These results are consistent with Eq. 1, indicating that the experimental design can accurately discriminate between solution concentrations in the donor chamber. Supersaturated solutions generated via dissolution of the three solid amorphous systems yielded slopes of 8.5 for the pure amorphous solid, 9.5 for 50:50, and 10.5 for the 90:10 (HPMC–felodipine) ASD. The theoretically estimated solubility for pure amorphous felodipine at 37°C is about 9 μg/mL or a factor of nine times that of the crystalline solubility. On the basis of calculated diffusion rate ratios, the dissolution of both pure amorphous felodipine and the solid dispersions generated solution concentrations (or more correctly solution activities) remarkably close to values predicted by Eq. 2, which provides a theoretical estimate for the pure amorphous material. This indicates that, at least over the timeframe that these experiments were conducted, there is no significant difference in the maximum thermodynamic activity of dissolved felodipine for solutions derived from the three amorphous systems. Additionally, this technique confirms that felodipine was not complexed with HPMC in the bulk solution as has been demonstrated in other systems under similar conditions.[26,27] On the basis of the measured concentrations from the UV probe experiments (Fig. 3), it would be expected that the diffusion rate of the 90% HPMC system would be at least twice that of the 50% HPMC and pure amorphous systems in direct contradiction to these experimental results. The diffusion data were supported by the NMR experiments, wherein the integrated peak area for the 90% HPMC solid dispersion sample was 1370 and the area for the 50% HPMC sample was 1014 arbitrary units, which was a relative difference of approximately 26%.

Indomethacin and PVP Dispersions

In order to test the generality of the above observations in different polymer–API solid dispersions, similar experiments were conducted using ASDs composed of indomethacin and PVP as well as indomethacin and HPMC (data not shown). Figure 12 shows the concentration–time profiles obtained at 25°C for 90:10 PVP–indomethacin and 50:50 PVP–indomethacin ASDs. As observed for felodipine, when the polymer content was 90%, elevated supersaturations appear to be generated as compared with the 50:50 sample (note the equilibrium crystalline solubility is ~1.2 μg/mL). The peak solution concentration generated in the 50:50 PVP–indomethacin solid dispersion was around 22 μg/mL, which was near the theoretically predicted value of 21 μg/mL for pure amorphous indomethacin in a buffered solution of pH 2.0, where no ionization would be expected. In contrast, the UV data indicate that the 90:10 (PVP–indomethacin) dispersion reached a maximum apparent solution concentration more than twice of the predicted amorphous solubility. For the 90% PVP solid dispersion, the solution became cloudy after addition to the buffer similar to the high polymer concentration felodipine dispersions. DLS was used to measure the size of the small particles present in these

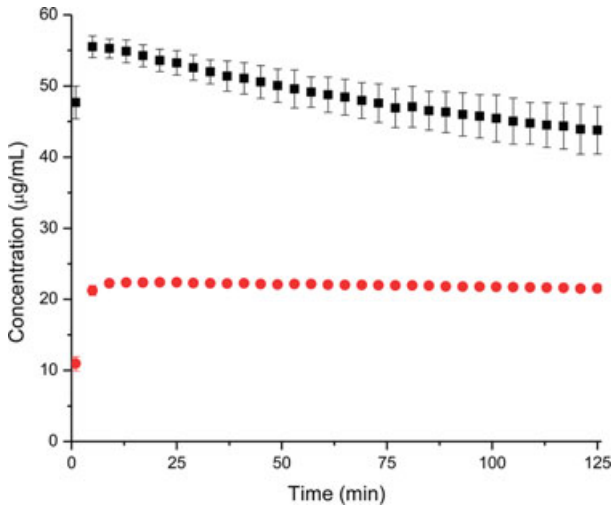

Figure 12. Apparent concentration–time profiles for dissolution of a 90:10 (■) and a 50:50 (●) PVP–indomethacin solid dispersion at 25°C. Error bars represent 1 standard deviation ($n = 3$).

suspensions. The presence of large dissolving particles for the first 25 min of the dissolution experiment prevented meaningful data from being collected (due to a poor correlation function). However, at 30 and 45 min, the concentration of large particles was low enough to make proper estimates of the average particle diameter, which were 210 and 217 nm, respectively. Similar to felodipine, uniform cloudiness was not observed with the 50:50 samples. As a result, a proper correlation function was not obtained at any time point with the 50:50 ASD presumably due to the absence of submicron particles.

Dissolution of the HPMC–indomethacin solid dispersions yielded profiles consistent with all other systems investigated in this paper. The 50:50 HPMC–indomethacin solid dispersion yielded a concentration–time profile similar to 50:50 PVP–indomethacin, wherein the peak solution concentration was near the effective solubility of neat amorphous indomethacin (~21 μg/mL). Dissolution of the 90:10 HPMC–indomethacin solid dispersion resulted in apparent solution concentrations five times greater than the 50:50 (HPMC–indomethacin) system. Again, this was consistent with all other systems containing 90% polymer investigated in this study. However, these systems produced apparent solution concentrations that were quite variable, fluctuating between 80 and 120 μg/mL. The absorbance at these concentrations was near the upper limit of linearity of the UV fiber optic system used for the experiments, which most likely explains the fluctuations in the experimental measurements.

DISCUSSION

The behavior of ASDs during dissolution is known to be extremely complex, with many processes taking place simultaneously.[17,28,29] From the UV experiments described above, dissolution of both felodipine and indomethacin ADSs containing 90% polymer (HPMC or PVP) apparently generated solutions with drug concentrations well in excess of those observed for the corresponding ASDs containing 50% polymer or the pure amorphous API. Additionally, the apparent maximum solution concentrations observed were much higher than the theoretical estimates for the pure amorphous form (Eqs. 2 and 3). In other words, according to the dissolution data obtained via the UV system, it appears at first glance that the 90:10 ASDs have the ability to generate much higher supersaturation ratios (where supersaturation ratio is defined as the ratio of the observed solution concentration to the crystalline equilibrium solubility) relative to the 50:50 ADSs regardless of which polymer or API is investigated. However, these results are in direct contradiction with the conclusions made from the diffusion and NMR studies. In these experiments, the data indicated that the peak concentrations of felodipine were similar for solutions produced by dissolution of the 90% HPMC and 50% HPMC ASDs, the neat amorphous solid, as well as the artificially created supersaturated solution of approximately 10 μg/mL. The most likely explanation for this discrepancy is the presence of the submicron particles (detected by the DLS measurements, see Figs. 6–9) generated during dissolution of the 90:10 ASDs. Although second derivatives of the spectra were taken in order to mitigate particle scattering effects,[30–33] very small particles on the order of the size seen in the DLS experiments (200–400 nm) can absorb light in a similar manner to the corresponding solution.[34] In a recent study, it has been noted that absorption of UV light by crystalline nanosupensions of felodipine occurs and is dependent on the amount of solid present in that suspension.[35] It was further noted that absorption by these small particulates leads to erroneous estimates of the solution concentration (solution concentration was estimated to be higher than that actually present). UV absorption by nanoparticles in solution is not corrected for by taking a second derivative, meaning that accurate concentration measurements cannot be easily performed by this technique in the presence of these submicron particles. The extent of absorption by particulates is strongly dependent on particle size over the nanometer size range and as particle size decreases, absorption efficiency relative to scattering efficiency increases dramatically.[34] This observation is relevant because in the current study the initially observed particle size (~200 nm) is small enough that a substantial degree of absorption would be anticipated. With this in mind, it is reasonable to hypothesize that the concentration estimates for the dissolution of the 90:10 dispersions derived from the UV fiber optic probe sampling methodology represent absorption not only from molecules in solution but also by molecules present in small particles. In contrast, both the diffusion and the NMR experiments measure only highly mobile species and therefore do not detect the molecules present as particulates.

It is of interest to consider further the difference in the dissolution behavior of the 90:10 and the 50:50 systems. The 90:10 HPMC–felodipine ASDs dissolved immediately upon exposure to dissolution buffer (see microscope images in Fig. 4), followed by the immediate formation of submicron particles (<5 min). In contrast, the 50:50 HPMC–felodipine ASD particles maintained their integrity and no submicron particles could be detected with the DLS measurements. Although the diffusion and NMR results suggested that the solution concentrations were the same for each system, neither experiment was able to provide information about the kinetics of the dissolution process because both techniques required data to be collected over at least a 40-min period.

Therefore, the generation of a short-lived, elevated solution concentration (most likely on a local scale) in the case of the 90:10 HPMC–felodipine dispersion cannot be discounted, and would in fact provide an explanation for the generation of the submicron particles observed. According to classical crystallization theory, the nucleation rate increases with increasing supersaturation. Spontaneous nucleation from solution occurs when the system reaches a sufficiently high level of supersaturation and is followed by crystal growth. Therefore, it might be anticipated that upon dissolution of a 90:10 ASD (HPMC, PVP–felodipine, or indomethacin), a highly supersaturated solution would be formed creating ideal conditions for rapid nucleation. We speculate that for the 90:10 ASDs, almost all of the drug present in the ASD particles rapidly dissolves into the solution forming a highly supersaturated state, from which it immediately begins to crystallize. This supposition is supported by the results of the DLS study, which shows that the submicron particulates generated upon dissolution of the 90:10 HPMC–felodipine ASD are not only similar in initial size to those derived from an artificially generated supersaturated solution but also grow at the same rate (Fig. 7). Again, these particles were not observed in the 50% HPMC experiments visually or by DLS. For the predissolved felodipine used to create the artificially supersaturated solutions, obviously all of the felodipine originates from the solution phase. On addition of this methanolic solution to buffer to create a supersaturation ratio of 60 (at 25°C), a substantial amount of precipitation is to be expected given the extremely high level of supersaturation. This precipitation clearly occurs, even in the presence of a predissolved crystallization inhibitor (HPMC), indicating that nucleation cannot be completely suppressed at this level of supersaturation. The fact that the behavior of the submicron precipitates was similar regardless of how they were created suggests that the mechanism of particle formation was similar for the ASDs and the artificially supersaturated solutions. It is interesting to note that the submicron particles produced at a supersaturation ratio of 60 grow much more rapidly in the absence of predissolved HPMC (Fig. 8), consistent with previous results demonstrating that HPMC is able to reduce the crystallization rate of felodipine from solution.[10]

The precipitates are thought to be crystalline rather than amorphous for the following reasons: First, they increase in size continuously with time and as they reach about 1 μm become visible as single (i.e., not aggregated) birefringent particles under polarized light microscopy (data not shown). Second, amorphous felodipine crystallizes rapidly on its own when exposed to aqueous solutions even in the presence of polymeric crystallization inhibitors.[10] In addition, evidence supporting our claim that these

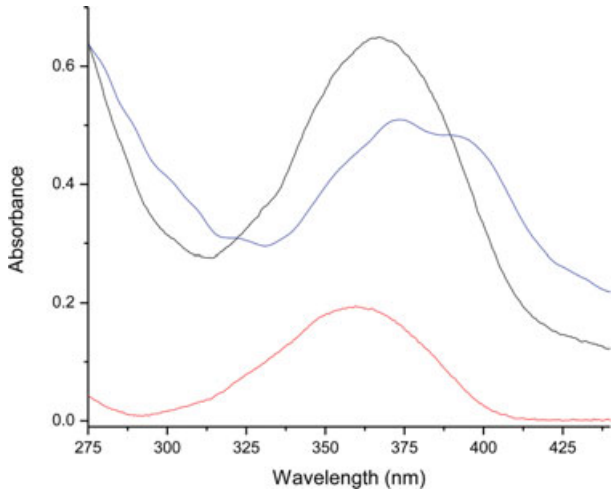

Figure 13. UV Absorption spectra of a 10 μg/mL methanolic solution of felodipine (red), 25 μg/mL solid content nanosuspension of felodipine (blue),[36] and a spectrum from the 90:10 (black) solid dispersion dissolution experiments at 60 min shown in Figure 2.

nanoparticles are crystalline can be found by analyzing the UV spectra of three different felodipine samples (Fig. 13)[36]: a spectrum obtained with the *in situ* UV probe after 60 min of dissolution of the 90:10 HPMC–felodipine ASDs (Fig. 2), wherein the apparent solution concentration is well above the amorphous solubility advantage; a spectrum of a methanolic solution of felodipine (10 μg/mL); and a spectrum of an aqueous crystalline nanosuspension of felodipine at 25 μg/mL solid content. The spectrum of felodipine in the methanolic solution has a peak at 360 nm and a valley at 294 nm, both of which are almost identical to the peaks and valleys obtained from spectra of felodipine as an amorphous film with thickness ranging from 1.5 μm down to 200 nm (data not shown). Felodipine dissolved in buffer has a slightly shifted peak at about 364 nm and a valley in the same position as the other two examples at 294 nm (data not shown). The spectrum of the crystalline nanosuspension is quite different, with the most important distinction coming from the significant red shift of the valley (325 nm) accompanied by a smaller shift in the peak (373 nm). When the spectrum from the dissolution experiment of the 90:10 HPMC–felodipine solid dispersion is compared with the solution and (predominantly) crystalline reference spectra, the peak (367 nm) and the valley (312 nm) are found at a position intermediate to the two control samples suggesting that this spectrum represents the combined absorption of felodipine dissolved in solution as well as absorption by crystalline nanoparticles. This spectral shift was observed within 5 min of the start of the dissolution of the 90:10 ASDs, which is consistent with the timeframe in which the particles were observed in the DLS experiments. It

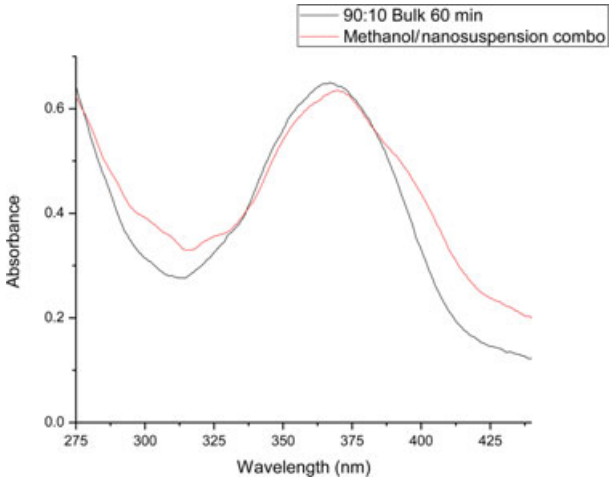

Figure 14. Summed UV Absorption spectra of the 10 μg/mL methanolic solution combined with the 25 μg/mL solid content nanosuspension of felodipine (Fig. 13) and a spectrum from the 90:10 solid dispersion dissolution experiments at 60 min (same spectrum as shown in Fig. 13). The combined spectrum from the methanol solution and the nanosuspension was uniformly reduced by 10% at all wavelengths so that the peak absorbance values for both spectra shown above were of the same magnitude.

should be noted that the red shift was not observed at any time point for solutions derived from dissolution of the 50:50 HPMC–felodipine ADS, pure amorphous system, or the 5 and 10 μg/mL control experiments (Fig. 10), supporting the conclusion that crystalline nanoparticles were only created during dissolution of the 90:10 HPMC–felodipine solid dispersions. As UV absorption is additive, combining the spectra of the solution and nanocrystalline felodipine samples should yield a spectrum similar to that obtained from the dissolved 90:10 HPMC–felodipine solid dispersion if our speculation is correct. As shown in Figure 14, the resultant additive spectrum shows a peak and valley in positions similar to those of the spectrum from the 90% HPMC ASD dissolution experiment. As felodipine dissolved in solution as well as amorphous films of felodipine do not demonstrate a significant red shift (small shift in peak of aqueous solution is noted above), it would be reasonable to conclude that the nanoparticles present in the systems following dissolution of 90:10 HPMC–felodipine ASDs were indeed crystalline. The possibility that the particles could originate from crystallization of small (i.e., nanometer scale) regions of amorphous drug present dispersed in the polymeric matrix cannot be entirely ruled out but seems unlikely given the high polymer concentration and the known molecular level miscibility of the systems in our investigation.[21–23]

The difference in the observed dissolution behavior of ASDs containing 50% versus 90% polymer is perhaps unsurprising, given the substantial body of evidence in the literature illustrating that the dissolution rate of an ASD depends on the drug–polymer ratio, although there is little information about the generation of submicron particles observed in our studies *per se.* At least two dissolution regimens, namely polymer controlled (high-polymer concentrations) and drug controlled (high-drug loadings) have been defined.[4,37,38] In some of the earliest studies on solid dispersions, Simonelli et al. compared the relative dissolution rates of amorphous dispersions of PVP and sulfathiazole. They observed that at high-drug loadings, although the initial dissolution rate was faster than that for the crystalline material, it did not depend on the polymer concentration (up to 50 wt % polymer). The authors concluded that, at a moderate to high drug loading, a relatively water-soluble polymer will dissolve into the bulk phase from the surface at a faster rate than the drug.[4] This will leave behind a drug-rich interface, possibly in the amorphous state, that regulates the dissolution rate of the remaining solid. At high-polymer loadings however, the dissolution rate of the drug was higher and congruent with the dissolution rate of the polymer, indicating that the polymer dissolution controlled the dissolution rate of the drug. At this elevated polymer loading, there would not be enough API present to physically form a drug-rich layer limiting dissolution.[37] Thus, in this regimen, the dissolution rate of the drug can be modeled as a fraction of the dissolution rate of the polymer by the relation shown in Eq. 4 below[4,37,39]:

$$G_D = \frac{G_C \times A_D}{A_C} \tag{4}$$

where G is the dissolution rate, A is the component concentration and the subscripts D and C refer to the drug and carrier, respectively. From a qualitative standpoint, the above observations indicate that the dissolution rate at very high-polymer concentration for a molecularly dispersed system of amorphous drug and polymer would be controlled by the dissolution rate of the polymer. The data presented for both felodipine and indomethacin appears to agree with this model where the dissolution rate of solid dispersions containing 90% polymer dissolved much faster than those with 50% polymer (Figs. 4, 5, and 12). This model provides a basis for our conclusion that 90:10 ASDs can generate very high local supersaturations directly controlled by the rapid dissolution of the polymer. For the 50:50 ASDs, supersaturations beyond those observable for the pure amorphous solid would not be expected because the dissolution behavior is controlled by a layer of pure drug. In other words, at the interface with the solution, the polymer has already entered the solution phase before the drug

dissolves and so the maximum solution concentration cannot exceed that of the pure drug.

A thermodynamic argument can be also made to explain the observed differences in dissolution behavior of the various solid dispersions investigated. The higher apparent solubility of a pure amorphous drug stems from the higher activity of the solid amorphous material where the ratio of the amorphous–crystalline solubilities is given by Eq. 2. On the basis of the diffusion results presented above, the ratio of the flux for the solution generated by the amorphous to that generated by the crystalline is close to what is estimated based on the activity differences between the drug in the crystalline and amorphous states. However, if the drug is present in an ASD, the activity of the drug would not be expected to be the same as in the pure amorphous solid; if miscibility has been achieved, the free energy of the system will be lower and consequently the activity of the drug in the dispersion will be lower than for the pure amorphous solid.[40–43] On the basis of this reasoning, the solubility advantage of a miscible amorphous dispersion might actually be expected to be lower using Eq. 2. However, an underlying assumption of Eq. 2 is that the solute–solvent interaction upon dissolution is the same for both solid forms (e.g., crystalline and amorphous). Although this assumption is quite reasonable when comparing the crystalline and pure amorphous forms, it is unlikely to be true when considering an ASD. Considering this from a thermodynamic standpoint, because the intermolecular bonding in the matrix of an ASD is different from that in a pure amorphous material, both the entropy and enthalpy of solution will be different between the two systems. This in turn results in differences in the energy required to bring the drug from the solid phase into the solution phase. Ignoring heat capacity contributions, the activity of a solute in solution is related to its solid phase by[44]

$$\ln \gamma c = \frac{\Delta H_f \times T_m}{R} \times \left(\frac{1}{T_m} - \frac{1}{T}\right) \tag{5}$$

where

$$\ln \gamma c = \ln a \tag{6}$$

where a is the activity, γ is the activity coefficient, c is the equilibrium solubility of the solute, ΔH_f is the enthalpy of fusion, R is the universal gas constant, T_m is the melting temperature, and T is the temperature of interest. This right hand side of the equation estimates the difference in free energy of the drug from a given physical form (usually the stable crystal) to its liquid form at a temperature T (i.e., energy of the crystal lattice). Removal of the energy barrier present in the crystal lattice leads to the origin of the solubility advantage for amorphous materials. An inherent assumption of this estimation is that γ is same for both the amorphous and crystalline form (aforementioned assumption in Eq. 2). This approach is derived from regular solution theory where γ represents the net energy required to mix the solvent (water in our case) with the solute in a pure liquid state. However, when the dissolving solid is composed of an API molecularly dispersed in a polymeric matrix, the free energy (and enthalpy) of solution would be different from that of the API in the pure state. Consequently, γ would not be expected to be the same for a miscible ASD. In both cases, the γ term represents the nonideality of mixing two different molecules defined by a nonzero enthalpy of solution (ΔH_{sol}). From an entropic standpoint, it is almost always favorable to introduce an additional component into a mixture.[45,46] From an enthalpic standpoint, ΔH_{sol} can either promote or prevent mixing and for a two-component system (i.e., pure amorphous system and water) is mathematically represented by Eq. 7,[47]:

$$\Delta H_{sol} = RT\chi_{12} n_1 V_2 \tag{7}$$

For a three-component system (ASD mixing with water):

$$\Delta H_{sol} = RT(n_1 V_2 \chi_{12} + n_1 V_3 \chi_{13} + n_2 V_3 \chi_{23}) \tag{8}$$

where χ is the binary interaction parameter between any two components, n is the mole fraction, and V is the volume fraction of a given component. The subscripts 1, 2, and 3 represent the water, drug, and polymer, respectively. These equations clearly show that the energetic exchange required to take place in order to remove a drug molecule from the solid phase to the solution phase is different in the pure amorphous form when compared with being dispersed in a polymeric matrix. In the case of the pure amorphous system, only the energy exchange between the solvent and API is considered. When a third component (i.e., polymer) is incorporated into the mixture, the energetic exchange of all three components must be considered. With respect to the drug and polymer, the relative amounts of these two components could have a significant impact on the ΔH_{sol}. In a miscible system where the amount of polymer is upward of 90% of the solid, the amount of potential drug–drug interactions in the solid will be significantly reduced compared with a system containing 50% polymer. As the drug–drug interactions resist solubilization and are in large part what dictate the value of χ_{12}, a reduction in these interactions would lead to a reduction in the barrier to the API entering the solution phase. It is helpful to consider that χ_{12} (where 2 in the binary mixture could be the drug or polymer) for the binary mixture in Eq. 7 would not be the same as χ_{12} for

the ternary mixture in Eq. 8, which makes practical application of Eq. 8 difficult. This stems from the fact that the interaction of the drug (or polymer) with water in the pure state is not necessarily the same when it is molecularly mixed with a second component as in an ASD.[48,49] Rumondor et al.[50] demonstrated that the interaction parameters measured for binary mixtures of felodipine and water and PVP and water could not be used with the ternary form of the Flory–Huggins model to obtain reasonable values for the interaction parameter between felodipine and PVP (χ_{23}). This was a result of the fact that the interaction of the drug (or polymer) and water is not the same in a solid dispersion as when it is in the pure state.

In summary, from a purely thermodynamic perspective, there is no reason to expect that the activity of a solution derived from an ASD would be the same as from the pure amorphous solid. Despite this thermodynamic reasoning, the diffusion experiments indicate that the activities in solution are in fact the same. It is easiest to rationalize this result for the 50:50 HPMC–felodpine dispersion based on the expected development of a drug-rich layer at the diffusion front, as a consequence of the faster dissolution rate of the polymer relative to the drug (see Simonelli et al.,[4] Corrigan,[37] and Craig[17] for a detailed discussion of this phenomenon). If this layer remains amorphous, then it would presumably control the solution concentration achieved. For the 90:10 HPMC–felodipine ASD, we rationalize that a higher solution concentration evolved through polymer controlled dissolution of the drug. This process was extremely fast and most likely local to the dissolving particles, whereby the resultant solute concentration was depleted by the rapid precipitation of submicron drug particles to the point where the solution activity is approximately the same as that generated from the pure amorphous solid. The fact that these values are similar may be purely coincidental (at this point we see no theoretical reason why they should be) and requires further investigation.

CONCLUSIONS

It is clear from the experimental results and analysis in this study that understanding the behavior of ASDs during dissolution requires knowledge of many different parameters. The amount of polymer relative to drug has a significant impact on the dissolution behavior of ASDs during dissolution. At moderate drug loading (50%), the solubility advantage of the solid dispersions was shown to be similar to that of pure amorphous system. This is a consequence of the difference in solubility between the drug and the polymer, which most likely leads to a drug-rich layer at the dissolving surface. At low-drug loading (10%), the solubility advantage was also shown to be similar to that of pure amorphous system as confirmed by diffusion and NMR experiments. At this drug loading, dissolution appeared to be controlled by the physicochemical properties of the polymer and resulted in a highly supersaturated solution from which felodipine immediately crystallized. This rapid precipitation generated submicron particles that prevented the accurate measurement of solution concentration via *in situ* UV spectroscopy as demonstrated by the diffusion and NMR experiments. The impact of this behavior on the *in vivo* performance of these systems is not clear at this point and will require further investigation.

ACKNOWLEDGMENTS

We would like to acknowledge PhRMA foundation for financial support for David E. Alonzo, as well as research funding from Abbott Laboratories. A special thanks to Kevin Boksa and Rushabh Sharma for their help in the laboratory.

REFERENCES

1. Hancock BC, Parks M. 2000. What is the true solubility advantage for amorphous pharmaceuticals? Pharm Res 17(4):397–404.
2. Konno H, Handa T, Alonzo DE, Taylor LS. 2008. Effect of polymer type on the dissolution profile of amorphous solid dispersions containing felodipine. Eur J Pharm Biopharm 70(2):493–499.
3. Leuner C, Dressman J. 2000. Improving drug solubility for oral delivery using solid dispersions. Eur J Pharm Biopharm 50(1):47–60.
4. Simonelli AP, Mehta SC, Higuchi WI. 1969. Dissolution rates of high energy polyvinylpyrrolidone (pvp)-sulfathiazole coprecipitates. J Pharm Sci 58(5):538–549.
5. Chen Y, Zhang GGZ, Neilly J, Marsh K, Mawhinney D, Sanzgiri YD. 2004. Enhancing the bioavailability of ABT-963 using solid dispersion containing Pluronic F-68. Int J Pharm 286(1–2):69–80.
6. DiNunzio JC, Miller DA, Yang W, McGinity JW, Williams RO. 2008. Amorphous cmpositions using concentration enhancing polymers for improved bioavailability of itraconazole. Mol Pharm 5(6):968–980.
7. Kennedy M, Hu J, Gao P, Li L, Ali-Reynolds A, Chal B, Gupta V, Ma C, Mahajan N, Akrami A, Surapaneni S. 2008. Enhanced bioavailability of a poorly soluble VR1 antagonist using an amorphous solid dispersion approach: A case study. Mol Pharm 5(6):981–993.
8. Law D, Schmitt EA, Marsh KC, Everitt EA, Wang WL, Fort JJ, Krill SL, Qiu YH. 2004. Ritonavir-PEG 8000 amorphous solid dispersions: *In vitro* and *in vivo* evaluations. J Pharm Sci 93(3):563–570.
9. Vaughn JM, McConville JT, Crisp MT, Johnston KP, Williams RO. 2006. Supersaturation produces high bioavailability of amorphous danazol particles formed by evaporative precipitation into aqueous solution and spray freezing into liquid technologies. Drug Dev Ind Pharm 32(5):559–567.
10. Alonzo DE, Zhang GGZ, Zhou DL, Gao Y, Taylor LS. 2010. Understanding the behavior of amorphous pharmaceutical systems during dissolution. Pharm Res 27(4):608–618.
11. Murdande SB, Pikal MJ, Shanker RM, Bogner RH. 2009 Solubility advantage of amorphous pharmaceuticals: I. A Thermodynamic analysis. J Pharm Sci 99(3):1254–1264.

12. Murdande SB, Pikal MJ, Shanker R, Bogner RH. 2011 Aqueous solubility of crystalline and amorphous drugs: Challenges in measurement. Pharm Dev Technol. 16**(3)**:187–200
13. Hoffman JD. 1958. Thermodynamic driving force in nucleation and growth processes. J Chem Phys 29(5):1192–1193.
14. Marsac PJ, Konno H, Taylor LS. 2006. A comparison of the physical stability of amorphous felodipine and nifedipine systems. Pharm Res 23(10):2306–2316.
15. Matteucci ME, Miller MA, Williams RO, Johnston KP. 2008. Highly supersaturated solutions of amorphous drugs approaching predictions from configurational thermodynamic properties. J Phys Chem B 112(51):16675–16681.
16. Verreck G, Six K, Van den Mooter G, Baert L, Peeters J, Brewster ME. 2003. Characterization of solid dispersions of itraconazole and hydroxypropylmethylcellulose prepared by melt extrusion—Part I. Int J Pharm 251(1–2):165–174.
17. Craig DQM. 2002. The mechanisms of drug release from solid dispersions in water-soluble polymers. Int J Pharm 231(2):131–144.
18. Serajuddin ATM. 1999. Solid dispersion of poorly water-soluble drugs: Early promises, subsequent problems, and recent breakthroughs. J Pharm Sci 88(10):1058–1066.
19. Gupta P, Kakumanu VK, Bansal AK. 2004. Stability and solubility of celecoxib-PVP amorphous dispersions: A molecular perspective. Pharm Res 21(10):1762–1769.
20. Patel R, Patel M. 2008. Preparation, characterization, and dissolution behavior of a solid dispersion of Simvastatin with polyethylene glycol 4000 and polyvinylpyrrolidone K30. J Dispersion Sci Technol 29:193–204.
21. Konno H, Taylor LS. 2006. Influence of different polymers on the crystallization tendency of molecularly dispersed amorphous felodipine. J Pharm Sci 95(12):2692–2705.
22. Yoshioka M, Hancock BC, Zografi G. 1995. Inhibition of indomethacin crystallization in poly(vinylpyrrolidone) coprecipitates. J Pharm Sci 84(8):983–986.
23. Taylor LS, Zografi G. 1997. Spectroscopic characterization of interactions between PVP and indomethacin in amorphous molecular dispersions. Pharm Res 14(12):1691–1698.
24. Wijmans JG, Baker RW. 1995. The solution-diffusion model—A review. J Membrane Sci 107(1–2):1–21.
25. Holzgrabe U. 2010. Quantitative NMR spectroscopy in pharmaceutical applications. Prog Nucl Magn Reson Spectrosc 57(2):229–240.
26. Corrigan OI, Farvar MA, Higuchi WI. 1980. Drug membrane-transport enhancement using high-energy drug polyvinylpyrrolidone (pvp) co-precipitates. Int J Pharm 5(3):229–238.
27. Hasegawa A, Taguchi M, Suzuki R, Miyata T, Nakagawa H, Sugimoto I. 1988. Supersaturation mechanism of drugs from solid dispersions with enteric coating agents. Chem Pharm Bull 36(12):4941–4950.
28. Doherty C, York P. 1987. Mechanisms of dissolution of frusemide PVP solid dispersions. Int J Pharm 34(3):197–205.
29. Simonelli AP, Mehta SC, Higuchi WI. 1976. Dissolution rates of high-energy sulfathiazole-povidone coprecipitates.2. Characterization of form of drug controlling its dissolution rate via solubility studies. J Pharm Sci 65(3):355–361.
30. Bynum K, Roinestad K, Kassis A, Pocreva J, Gehrlein L, Cheng FPP. 2001. Analytical performance of a fiber optic probe dissolution system. Dissolution Technol 8(4):1–10.
31. Liu L, Fitzgerald G, Embry M, Cantu R, Pack B. 2008. Technical evaluation of a fiber-optic probe dissolution system. Dissolution Technol 15(1):10–20.
32. Mirza T, Liu Q, Vivilecchia R, Joshi Y. 2009. Comprehensive validation scheme for *in situ* fiber optics dissolution method for pharmaceutical drug product testing. J Pharm Sci 98(3):1086–1094.
33. Schatz C, Ulmschneider M, Altermatt R, Marrer S, Altorfer H. 2001. Thoughts on fiber optics in dissolution testing. Dissolution Technol 8(2):1–5.
34. Bohren CF, Huffman DR. 1983. Absorption and scattering of light by small particles. 1st ed. New York: John Wiley & Sons.
35. van Eerdenbrugh B, Alonzo DE, Taylor LS. 2011. Influence of particle size on the ultraviolet spectrum of particulate-containing solutions—Implications for in-situ concentration monitoring using UV/Vis fiber-optic probes. Pharm Res. DOI: 10.1007/s11095-011-0399-4.
36. Alonzo DE. 2010. Maximizing the solubility advantage of amorphous pharmaceutical systems. Industrial and physical pharmacy.West Lafyayette: Purdue University, pp 168.
37. Corrigan OI. 1985. Mechanisms of dissolution of fast release solid dispersions. Drug Dev Ind Pharm 11(2–3):697–724.
38. Corrigan OI. 1986. Retardation of polymeric carrier dissolution by dispersed drugs—Factors influencing the dissolution of solid dispersions containing polyethylene glycols. Drug Dev Ind Pharm 12(11–13):1777–1793.
39. Corrigan OI, Stanley CT. 1982. Mechanism of drug dissolution rate enhancement from beta-cyclodextrin-drug systems. J Pharm Pharmacol 34(10):621–626.
40. Thompson CV, Spaepen F. 1979. Approximation of the free-energy change on crystallization. Acta Metallurgica 27(12):1855–1859.
41. Marsac P, Li T, Taylor L. 2009. Estimation of drug-polymer miscibility and solubility in amorphous solid dispersions using experimentally determined interaction parameters. Pharm Res 26(1):139–151.
42. Tao J, Sun Y, Zhang GGZ, Yu L. 2009. Solubility of small-molecule crystals in polymers: d-Mannitol in PVP, indomethacin in PVP/VA, and nifedipine in PVP/VA. Pharm Res 26(4):855–864.
43. Marsac PJ, Shamblin SL, Taylor LS. 2006. Theoretical and practical approaches for prediction of drug-polymer miscibility and solubility. Pharm Res 23(10):2417–2426.
44. Nordstrom FL, Rasmuson AC. 2008. Determination of the activity of a molecular solute in saturated solution. J Chem Thermodyn 40(12):1684–1692.
45. Flory PJ.. 1953. Principles of polymer chemistry. 1st ed. Ithaca, New York: Cornell University Press.
46. Rajagopalan R, Hiemenz PC. 1997. Principals of colloid and surface chemistry. 3rd ed.Boca Raton: Taylor & Francis Group, LLC.
47. Zhang J, Zografi G. 2001. Water vapor absorption into amorphous sucrose-poly(vinyl pyrrolidone) and trehalose-poly(vinyl pyrrolidone) mixtures. J Pharm Sci 90(9):1375–1385.
48. Csaki KF, Nagy M, Csempesz F. 2005. Influence of the chain composition on the thermodynamic properties of binary and ternary polymer solutions. Langmuir 21(2):761–766.
49. Sabzi F, Boushehri A. 2006. Compatibility of polymer blends. I. Copolymers with organic solvents. J Appl Polym Sci 101(1):492–498.
50. Rumondor ACF, Konno H, Marsac PJ, Taylor LSAnalysis of the moisture sorption behavior of amorphous drug-polymer blends. J Appl Polym Sci 117(2):1055–1063.